NUCLEAR SCIENCE AND ENGINEERING: **164**, 87–104 (2010)

Daubechies' Wavelet Method for Angular Solution of the Neutron Transport Equation

Youqi Zheng, Hongchun Wu, and Liangzhi Cao

Xi'an Jiaotong University, School of Nuclear Science and Technology, Xi'an 710049, China

and

Nam Zin Cho*

Korea Advanced Institute of Science and Technology, Department of Nuclear and Quantum Engineering, Daejeon 305-701, Korea

Received March 3, 2009
Accepted June 28, 2009

Abstract—*This paper describes Daubechies' wavelet method (DWM) for the discretization of the angular variable in the neutron transport equation. Two special features are introduced: (a) the azimuthal angle is discretized using the Daubechies' scaling function as the basis function, while the polar angle is decoupled and discretized using the discrete ordinates in a standard manner, and (b) the construction of Daubechies' wavelets on an interval is used to get around the edge effect between subdomains in the angular variable. In addition, two acceleration methods, namely, coarse mesh rebalance and coarse mesh finite difference, are implemented in DWM. The test results on several benchmark problems indicate that DWM described in this paper is capable of treating transport problems exhibiting angularly complicated behaviors, effective in mitigating ray effect, and versatile in handling transport phenomena in a variety of structured media.*

I. INTRODUCTION

Over the past decades, many numerical methods have been developed to discretize the angular variable in the neutron transport equation, such as the discrete ordinates (S_N) method and the spherical harmonics (P_N) method. In recent years, some nonstandard angular discretization schemes have been developed, such as the spectral method using Walsh functions,[1] the Jacobi polynomial approximations based on Chebyshev polynomials (T_N) and ultraspherical (U_N) polynomials,[2] and the wavelet function method based on the lifting scheme.[3,4] In this study, we discretize the angular variable in the transport equation by using the Daubechies' wavelet function.[5] This Daubechies' wavelet method (DWM) is based on the normal tensor product form of angular space and uses the orthonormal wavelets as basis functions. Without the lifting scheme, this kind of wavelet basis can be used directly with a known orthonormal expression in the angular expansion. DWM is similar to the P_N method, but the basis functions are the Daubechies' scaling functions, which construct the wavelet functions. Another important difference is that the expansion of the angular variable is restricted locally, in the compact support of basis functions, rather than in an infinite and periodic space. The solution can also be expressed in continuous functional form, but the accuracy depends on the distribution of discrete scaling functions.

Wavelets and wavelet transforms were actively developed in the last two decades. Practical applications implementing wavelets are related to the Fourier and windowed Fourier transforms. The wavelet functions are generated by dilation and translation operations and have the powerful property of localization in space. This property may be utilized to describe the angular distribution accurately, especially for some irregular distributions

*E-mail: nzcho@kaist.ac.kr

discovered in recent investigations.[6,7] In this paper, the Daubechies' scaling functions, which were constructed in early 1990s, are selected as the basis functions.

This paper builds upon the previous works[8,9] for solving neutron transport problems and describes in detail the methodology of DWM. The tensor product form for the two-dimensional angular variable discretization is applied as an approximation to the exact spherical form. This form of angular definition is feasible for both normal two-dimensional wavelet expansion and decoupling of the angular variable discretizations in two directions. To make the methodology description complete, the basic theory of Daubechies' wavelets and their modified forms on the interval are given in detail in this paper, together with the approach of calculating wavelet function values. In this paper, a practical form of DWM is given, which is stable, accurate, and efficient. DWM is verified by comparing its solutions to those of the CRX code,[10] which is based on the method of characteristics (MOC). In addition to the source iteration scheme for the numerical solution of DWM, two acceleration methods, coarse mesh rebalance (CMR) and coarse mesh finite difference (CMFD), are implemented.

The paper is organized as follows. In Sec. II, the basic theory of wavelets, especially the Daubechies' wavelets, is given. Both the properties and the related calculations are described in this section. DWM is deduced in detail in Sec. III, resulting in the final form of the decoupled transport equation, in which the polar angle is treated in discrete ordinates and the azimuthal angle in the Daubechies' scaling function expansion, respectively. The acceleration methods, CMR and CMFD, are also formulated in this section. Several numerical tests are given in Sec. IV to demonstrate the capability of DWM. Finally, Sec. V provides the conclusions of the study.

II. FUNDAMENTALS OF WAVELET THEORY

II.A. The Concept of Wavelets

Wavelets were first implemented in the area of signal processing. The wavelet functions were translated and dilated from a single function, and the analysis was performed by using the wavelet functions to weight the integration of the signal. This process was named the wavelet transform.

The wavelet functions are defined by a dilation and translation operation such as

$$\psi_{n,k} = 2^{n/2}\psi(2^n x - k) \tag{1}$$

for some $\psi \in L^2(R)$ and $(n,k) \in Z^2$. Z and R denote the set of integers and real numbers. $L^2(R)$ denotes the space of measurable, square-integrable functions.

The wavelet functions are generated from the scaling functions $\phi_{n,k}(x)$, which have the same form

$$\phi_{n,k} = 2^{n/2}\phi(2^n x - k) \tag{2}$$

for some $\phi \in L^2(R)$. Suppose we define

$$V_n = closure\langle \phi_{n,k} : k \in Z \rangle \tag{3}$$

and

$$W_n = closure\langle \psi_{n,k} : k \in Z \rangle \ ; \tag{4}$$

then, the scaling functions and the wavelet functions have the following subspace relations:

$$\phi_{n,k} \in V_n \ , \tag{5}$$

$$\psi_{n,k} \in W_n \ , \tag{6}$$

$$\ldots V_{-1} \subset V_0 \subset V_1 \subset V_2 \ldots \ , \tag{7}$$

$$V_n = V_{n-1} \oplus W_{n-1} \ , \tag{8}$$

$$\overline{\bigcup_n V_n} = L^2(R) \ , \tag{9}$$

and

$$\oplus_n W_n = L^2(R) \ , \tag{10}$$

where $\oplus$ stands for orthogonal sum.

From Eq. (8), we have

$$V_n = V_{n-m} \oplus W_{n-m} \oplus \cdots \oplus W_{n-2} \oplus W_{n-1} \ . \tag{11}$$

Thus, a wavelet decomposition at scale n becomes

$$f_n(x) = f_{n-m}(x) + \sum_{j=n-m}^{n-1} g_j(x) \ , \quad f_j \in V_j \ , \quad g_j \in W_j \tag{12}$$

or

$$f_n(x) = \sum_k a_{n,k}\phi_{n,k}(x) = \sum_k a_{n-m,k}\phi_{n-m,k}(x) + \sum_{j=n-m}^{n-1}\sum_k b_{n-m,k}\psi_{j,k}(x) \ , \tag{13}$$

where $f_n(x)$ represents the function f at the single scale n. The second expression gives a representation of the function f in multiscale.

If we define $\phi \in V_0$, $\psi \in W_0$, and $V_1 = V_0 \oplus W_0$, the following two-scale relations hold:

$$\phi(x) = \sum_k c_k \phi(2x - k) \tag{14}$$

and

$$\psi(x) = \sum_k d_k \phi(2x - k) \ . \tag{15}$$

If the two-scale relation is restricted by finite sums, the scaling function and wavelet function have compact supports. In addition, if ψ is required to generate orthonormal bases, the relationship of expansion coefficients becomes

$$d_k = (-1)^k c_{1-k} \ . \tag{16}$$

As described above, various wavelets have been constructed according to the basic wavelet concept. Among them, the Daubechies' wavelets are employed in this study.

II.B. Definition and Properties of Daubechies' Wavelets

Daubechies discovered that it was possible to develop a wavelet with desired properties suitable to a specific problem. Based on the discrete wavelet transform, a new set of compactly supported orthonormal wavelets was constructed. They are named Daubechies' wavelets, for which the scaling functions $\phi_{n,k}(x)$ and wavelet functions $\psi_{n,k}(x)$ are represented as

$$\phi_{n,k}(x) = \sum_{j=2k}^{2N+2k-1} c_{j-2k}\phi_{n+1,j}(x) \tag{17}$$

and

$$\psi_{n,k}(x) = \sum_{j=2k-2N+2}^{2k-1} (-1)^j c_{1-j+2k}\phi_{n+1,j}(x) \ , \tag{18}$$

where n is called dilation order and N is called Daubechies order.

The Daubechies' wavelets, including both scaling functions and wavelet functions, have the following properties:

$$support\,\langle\phi_{n,k}(x)\rangle = [2^{-n}k, 2^{-n}(k+2N-1)] \ , \tag{19}$$

$$support\,\langle\psi_{n,k}(x)\rangle = [2^{-n}(k+1-N), 2^{-n}(k+N)] \ , \tag{20}$$

$$\phi_{n,k}, \psi_{n,k} \in C^{\lambda(N)} = \begin{array}{l}\text{space of Hölder continuous} \\ \text{functions with exponent}\end{array} \ , \tag{21}$$

$$\int \phi_{n,k}(x)\phi_{n,l}(x)\,dx = \delta_{kl} \ , \tag{22}$$

$$\int \psi_{n,k}(x)\psi_{m,l}(x)\,dx = \delta_{mn}\delta_{kl} \ , \tag{23}$$

and

$$\int \psi_{n,k}(x)x^m\,dx = 0 \ . \tag{24}$$

From Eqs. (19) and (20), we know that the supporting region is related to the dilation order n and Daubechies order N. Also, we know from Eq. (21) that a large Daubechies order N produces a smoother distribution of scaling functions and wavelet functions. Figure 1 shows the scaling function and its corresponding wavelet function for Daubechies order $N = 2$ and $N = 4$. The orthogonality conditions in Eqs. (22) and (23) are very important because they are the bases to pick up the individual moment from coupled expansion coefficients in the angular discretization. Equation (24) is the vanishing moments condition for the wavelets, which determines the Daubechies' coefficients c_k. The coefficients are calculated by multiresolution analysis. The details are available in Ref. 5. Therefore, only the results are taken from the reference. In Table I, the coefficients for Daubechies order $N = 2$ and $N = 4$ are given.

TABLE I

Coefficients c_k, $k = 1, \ldots, 2N-1$ for $N = 2$ and $N = 4$

	k	c_k
$N = 2$	0	0.482962913
	1	0.836516303
	2	0.224143868
	3	−0.129409522
$N = 4$	0	0.032223101
	1	−0.012603967
	2	−0.099219544
	3	0.297857796
	4	0.803738752
	5	0.497618668
	6	−0.029635528
	7	−0.075765715

II.C. The Daubechies' Wavelets on an Interval

To apply the Daubechies' scaling function to expand the angular variable, the basis functions are defined on an interval. Generally, a unit interval is considered without loss of generality. However, from Eq. (19), we find that the supporting region is related to the dilation order and Daubechies order, which makes them overlap the intervals. This requires a special treatment. Figure 2 illustrates the distribution of scaling functions on a unit interval for Daubechies order $N = 2$ and dilation order $n = 3$.

A technique to restrict the wavelets on an interval is to consider the "wrapped" wavelets,[11] which requires only simple transformation of known scaling functions and wavelet functions. It is a process of periodic transformation, which considers different contributions from translations and truncates the wavelets that overlap the interval periodically. Although it is simple to use, it requires the expanded functions to be periodic; i.e., it forces the values of the unknown functions to be equal at two

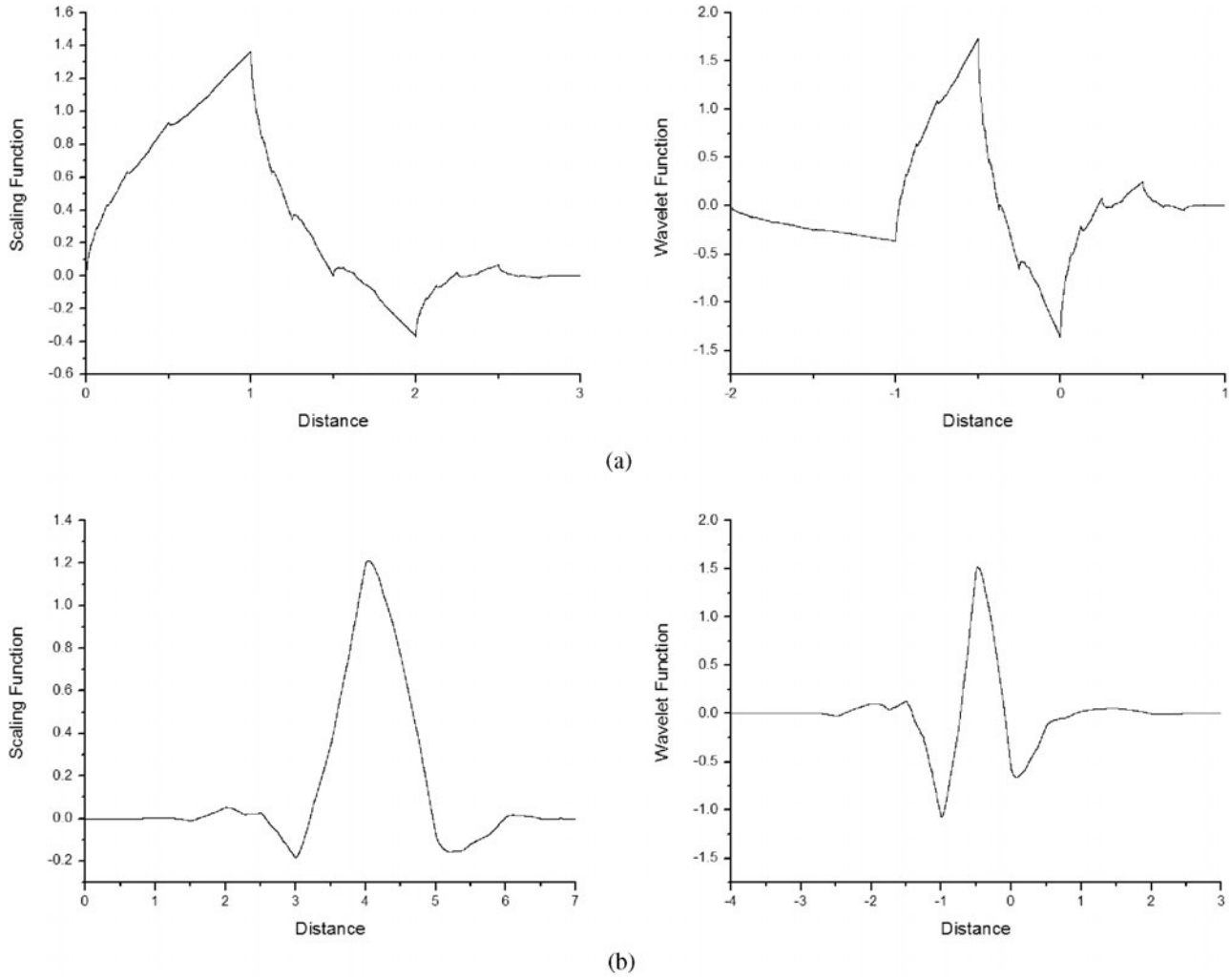

Fig. 1. Distribution of scaling function and wavelet function: (a) ($N = 2$) and (b) ($N = 4$).

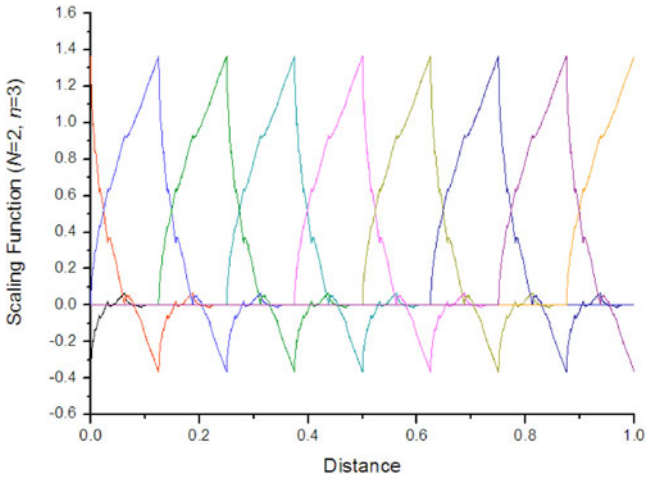

Fig. 2. Distribution of original scaling function for $N = 2$ and $n = 3$ on a unit interval.

edges. This phenomenon is called the edge effect. It may significantly change the values of unknown functions at the interface between two regions.

To avoid the edge effect, we use the Daubechies' wavelets on the interval constructed by Cohen, Daubechies, and Vial.[12] The main idea is to retain the wavelets inside the interval with the ones overlapping the interval removed. Then, the wavelets on the boundaries are constructed based on the fast wavelet transform. We start by illustrating the construction on the half line $[0,\infty)$ and assume the wavelets are supported on $[0,\infty)$.

Define the boundary scaling function for dilation order $n = 0$ as

$$\phi_0^{left}(x) = \sum_{k=-\infty}^{N-2} \phi(x-k) = \sum_{k=-N+1}^{N-2} \phi(x-k) \ ; \qquad (25)$$

TABLE II

Coefficients $H_{k,l}$, $h_{k,l}$, $G_{k,l}$, and $g_{k,l}$ for Left and Right Edges ($N = 2$)

		$H_{k,l}$ or $h_{k,l}$	$G_{k,l}$ or $g_{k,l}$			$H_{k,l}$ or $h_{k,l}$	$G_{k,l}$ or $g_{k,l}$
	l	Left Side			l	Right Side	
$k = 0$	0	0.60333	−0.79654	$k = -2$	−5	0.44315	0.23156
	1	0.69090	0.54639		−4	0.76756	0.40107
	2	−0.39831	−0.25879		−3	0.37496	−0.71758
$k = 1$	0	0.03752	0.01004		−2	0.19015	−0.36391
	1	0.45733	0.12235		−1	−0.19423	0.37172
	2	0.85009	0.22743	$k = -1$	−3	0.23039	−0.53982
	3	0.22382	−0.83660		−2	0.43490	0.80142
	4	−0.12922	0.48301		−1	0.87051	−0.25751

then, we know that the boundary scaling function has compact support and is orthogonal to all the interior scaling functions $\phi_{0,k}$. In the same way, we can also get the boundary scaling function ϕ_0^{right} on the other half line $(-\infty,0]$. The boundary scaling functions ϕ_0^{left}, ϕ_0^{right} and interior scaling functions $\phi_{0,k}$ (that are local inside the interval) are used to construct a new set of scaling functions, the Daubechies' scaling functions on the interval.

Usually, we expect there to be 2^n $(n > 0)$ scaling functions on the interval. This requires more than one boundary scaling function on each side, where the number is related to the Daubechies' order N; i.e., the boundary scaling functions are defined as $\phi_{n,k}^{left}$ and $\phi_{n,k}^{right}$ on the left and right sides with the index k standing for the integers in $[0, N-1]$ and $[-N, -1]$, respectively. Cohen, Daubechies, and Vial[12] proved that the following two-scale relations hold between Daubechies' wavelets on the interval:

$$\phi_{n,k}^{left} = \sum_{l=0}^{N-1} H_{k,l}^{left} \phi_{n+1,l}^{left} + \sum_{m=N}^{N+2k} h_{k,m}^{left} \phi_{n+1,m} \ , \tag{26}$$

$$\psi_{n,k}^{left} = \sum_{l=0}^{N-1} G_{k,l}^{left} \phi_{n+1,l}^{left} + \sum_{m=N}^{N+2k} g_{k,m}^{left} \phi_{n+1,m} \ , \tag{27}$$

$$\phi_{n,k}^{right} = \sum_{l=-N}^{-1} H_{k,l}^{right} \phi_{n+1,l}^{right} + \sum_{m=-N-1}^{-N-1+2k+2} h_{k,m}^{right} \phi_{n+1,m} \ , \tag{28}$$

and

$$\psi_{n,k}^{right} = \sum_{l=-N}^{-1} G_{k,l}^{right} \phi_{n+1,l}^{right} + \sum_{m=-N-1}^{-N-1+2k+2} g_{k,m}^{right} \phi_{n+1,m} \ , \tag{29}$$

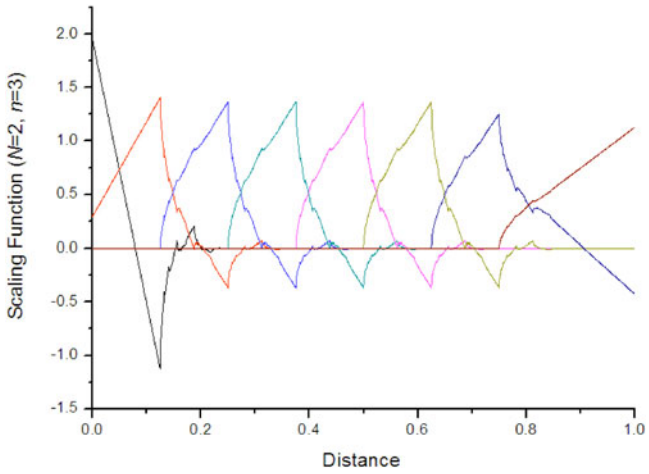

Fig. 3. Distribution of modified scaling function for $N = 2$ and $n = 3$ on a unit interval.

where

$\phi_{n,k}, \psi_{n,k}$ = scaling function and wavelet function, respectively

$H_{k,l}, h_{k,l}, G_{k,l}, g_{k,l}$ = filter coefficients constructed by Daubechies.

Table II shows some examples for H_{kl}, h_{kl}, G_{kl}, and g_{kl}. For Daubechies order $N = 2$ and dilation order $n = 3$, the distribution of the new scaling functions is illustrated in Fig. 3.

II.D. Related Calculations of Daubechies' Scaling Function

The basis functions are the starting point for the calculation of the Daubechies' scaling functions. Unfortunately, the Daubechies' scaling functions cannot be

expressed analytically. Therefore, discrete values of the scaling functions are generated by using the basic two-scale equation with known Daubechies' coefficients.

Here we take the calculation of $N = 2$ for an example. In this case, the number of c_k is four. Considering the values at the edges of the scaling functions being equal to zero, there are only two values to be determined as

$$\phi(1) = c_0\phi(2) + c_1\phi(1) \tag{30}$$

and

$$\phi(2) = c_2\phi(2) + c_3\phi(1) \ . \tag{31}$$

In matrix form they can be rewritten as

$$\Phi = L\Phi \ . \tag{32}$$

An iteration scheme is applied as

$$\Phi^{l+1} = L\Phi^{l} \ , \tag{33}$$

and the values of $\phi(x)$ at the integers are obtained by adding a normalization condition

$$\sum_k \phi(k) = 1 \ . \tag{34}$$

Then, we can get the values of the scaling function at other points recursively from Eq. (14). With the discrete values of the scaling function, we can directly calculate the values of the boundary functions at the integers and recursively generate the values at other points according to Eqs. (26) and (28). The values with fine refinements are required for the numerical integrations in Sec. III.

III. DAUBECHIES' WAVELET METHOD

III.A. Angular Discretization Scheme in DWM

In this paper, the neutron transport process is described by the following steady-state linear Boltzmann equation for the angular flux $\Phi(r, \Omega, E)$:

$$\Omega\nabla\Phi(r,\Omega,E) + \Sigma_t\Phi(r,\Omega,E) = q_f(r,\Omega,E) + q_s(r,\Omega,E) + q_{ex}(r,\Omega,E) \ , \tag{35}$$

where r, Ω, and E stand for the spatial, angular, and energy variables, respectively; q_f and q_s are the fission and scattering source terms:

$$q_f(r,\Omega,E) = \frac{\chi(E)}{4\pi k}\int_0^\infty\int_{4\pi}\nu\Sigma_f(r,E')\times\Phi(r,\Omega',E')\,d\Omega'\,dE' \tag{36}$$

and

$$q_s(r,\Omega,E) = \int_0^\infty\int_{4\pi}\Sigma_s(r,\Omega'\to\Omega,E'\to E)\times\Phi(r,\Omega',E')\,d\Omega'\,dE' \ , \tag{37}$$

where q_{ex} denotes the extra source term. All deductions are based on the Cartesian geometry and multigroup approximation for the energy treatment. To make it transparent in this paper, only the two-dimensional form is presented here (the three-dimensional form presents no essential difference). Then, the spatial and angular coordinates in the leakage operator are defined as

$$\Omega\cdot\nabla = (\Omega_x,\Omega_y)\cdot\left(\frac{\partial}{\partial x},\frac{\partial}{\partial y}\right) = \Omega_x\frac{\partial}{\partial x} + \Omega_y\frac{\partial}{\partial y} \ , \tag{38}$$

$$\Omega_x = (1-\mu^2)^{1/2}\cos\varphi \ , \tag{39}$$

and

$$\Omega_y = (1-\mu^2)^{1/2}\sin\varphi \ , \tag{40}$$

where μ is the polar cosine in the axial direction and φ is the azimuthal variable in the radial direction.

Generally, the angular variables are defined on the sphere with μ and φ. However, in the wavelet theory, the two-dimensional wavelet expansion is usually represented by using the tensor product form as

$$f(x,y) = \sum_k\sum_l f_{k,l}\phi_{n,k}(x)\phi_{n,l}(y) \ , \tag{41}$$

where $x = \mu$ and $y = \varphi$.

This form has been proved theoretically correct for high-dimensional bases of Daubechies' scaling functions and wavelet functions in the orthogonal spaces. In this study, the angular discretization derives from the same idea and assumes that the spherical angular variables can be represented in the orthogonal forms as

$$\Phi(r,\Omega,E) = \Phi_P(r,\mu,E)\otimes\Phi_A(r,\varphi,E) \ , \tag{42}$$

where Φ_P and Φ_A are defined as the individual tensor of angular flux with polar variable only and azimuthal variable only, respectively. Based on this, the two-dimensional expansion of angular flux is transformed to two one-dimensional expansions. Encouraged by our previous study,[9] we use the decoupled angular approach, in which the polar angle is treated in discrete ordinates (S_N discretization) and the azimuthal angle in Daubechies' scaling function expansion. This scheme has been demonstrated to be stable and accurate enough for the angular discretization of the linear transport equation.[9] Moreover, it is highly efficient and stable compared to the direct two-dimensional expansion form.

As with the P_N method, DWM suffers from the difficulties treating the boundary conditions. The double

P_N method[13] provides a means of expressing the boundary conditions exactly, which may be also used in DWM. A piecewise expansion of the angular flux is applied in the azimuthal direction, which we refer to as the angular subdomain scheme. This scheme consists of several subdomains in the azimuthal angular range at intervals of every 90 deg. Therefore, at the boundary, the incident and emergent angular fluxes are expressed separately, and the boundary conditions are represented in the exact form between the incident and emergent fluxes.

Based on the tensor product form of the angular flux and the angular subdomain scheme, a coordinate transformation must be performed in the angular definition. The scaling functions are restricted to a unit interval; therefore, substitutions of the angular variables are taken as

$$\Phi_g(r,\mu,\varphi) = \begin{cases} \Phi_g^1\left(r,\mu,-\pi+\dfrac{\pi}{2}\,\xi\right) \\ \Phi_g^2\left(r,\mu,-\dfrac{\pi}{2}\,\xi\right) \\ \Phi_g^3\left(r,\mu,\dfrac{\pi}{2}\,\xi\right) \\ \Phi_g^4\left(r,\mu,\pi-\dfrac{\pi}{2}\,\xi\right) \end{cases} , \tag{43}$$

where $\mu \in [0,1]$ and $\xi \in [0,1]$. Φ_g^1, Φ_g^2, Φ_g^3, and Φ_g^4 stand for the angular flux in the four quadrants of the upper hemisphere.

The angular discretization starts with the treatment of the polar variable, in which the discrete ordinates are applied. The fully symmetric Gaussian quadrature set is employed. We begin by integrating both sides of the neutron transport equation as follows:

$$\int d\mu\{(\Omega\nabla+\Sigma_t)\Phi_g(r,\mu,\varphi) - S_g(r,\mu,\varphi)\} = 0 \ , \tag{44}$$

where for brevity we rewrite the source terms in the form of $S_g(r,\mu,\varphi)$.

Define

$$\int_{\Delta\mu_m} \Phi_g(r,\mu,\varphi)\,d\mu = \omega_m \Phi_{g,m}(r,\varphi) \tag{45}$$

and

$$\int_{\Delta\mu_m} \Omega\nabla\Phi_g(r,\mu,\varphi)\,d\mu = \omega_m[\Omega\nabla\Phi_g(r,\mu,\varphi)]_m \ . \tag{46}$$

Then we obtain the following neutron transport equation with only the azimuthal variable remaining:

$$(\Omega_m\nabla+\Sigma_t)\Phi_{g,m}(r,\varphi) = S_{g,m}(r,\varphi) \ . \tag{47}$$

Now we use the Daubechies' scaling functions to expand the azimuthal variable as

$$\Phi_{g,m}(r,\Omega) = \sum_{p=1}^{P} \psi_{g,mp}(r)\phi_{n,p}(\varphi) \ , \tag{48}$$

where the set of $\phi_{n,p}$ consists of scaling functions inside the interval and on the boundaries at scale n. The P defines the total number of expansion coefficients (equal to 2^n). The Galerkin method is then applied to determine the expansion coefficients according to

$$\int \phi_{n,p'}(\varphi)\,d\varphi\left\{(\Omega_m\nabla+\Sigma_t)\sum_{p=1}^{P}\psi_{g,mp}(r)\phi_{n,p}(\varphi) - S_{g,m}(r,\varphi)\right\} = 0 \ , \tag{49}$$

and the final angular discretized form of the transport equation is given as follows:

$$\sum_{p=1}^{P}\left(D_{x,mpp'}\frac{\partial\psi_{g,mp}}{\partial x} + D_{y,mpp'}\frac{\partial\psi_{g,mp}}{\partial y}\right) + \Sigma_t\psi_{g,mp'} = S_{g,mp'} \ , \tag{50}$$

$$\begin{aligned} D_{x,mpp'} &= (1-\mu_m^2)^{1/2}\int \cos\varphi\cdot\phi_{n,p}(\varphi)\cdot\phi_{n,p'}(\varphi)\,d\varphi \\ &= 2^n(1-\mu_m^2)^{1/2}\int \cos\varphi\cdot\phi(2^n\varphi-p)\cdot\phi(2^n\varphi-p')\,d\varphi \ , \end{aligned} \tag{51}$$

$$\begin{aligned} D_{y,mpp'} &= (1-\mu_m^2)^{1/2}\int \sin\varphi\cdot\phi_{p}(\varphi)\cdot\phi_{p'}(\varphi)\,d\varphi \\ &= 2^n(1-\mu_m^2)^{1/2}\int \sin\varphi\cdot\phi(2^n\varphi-p)\cdot\phi(2^n\varphi-p')\,d\varphi \ , \end{aligned} \tag{52}$$

and

$$S_{g,mp'} = \int \phi_{p'}(\varphi) S_{g,m}(r,\varphi)\, d\varphi = 2^{n/2} \int \phi(2^n\varphi - p') \cdot S_{g,m}(r,\varphi)\, d\varphi \ , \tag{53}$$

where $D_{x,mpp'}$ and $D_{y,mpp'}$ denote transformations of the leakage operator at the given Gaussian quadrature (polar) point m. They are calculated using the discrete values of the Daubechies' scaling function given in Sec. II.D. The trapezoidal method is used for the integration:

$$D_{x,mpp'} = (1-\mu_m^2)^{1/2} \sum_{i=1}^{I} \frac{h}{2} [\cos\varphi_{i-1} \cdot \phi(2^n\varphi_{i-1} - p) \cdot \phi(2^n\varphi_{i-1} - p') + \cos\varphi_i \cdot \phi(2^n\varphi_i - p) \cdot \phi(2^n\varphi_i - p')] \ , \tag{54}$$

$$D_{x,mpp'} = 2^n(1-\mu_m^2)^{1/2} \sum_{i=1}^{I} \frac{h}{2} [\sin\varphi_{i-1} \cdot \phi(2^n\varphi_{i-1} - p) \cdot \phi(2^n\varphi_{i-1} - p') + \sin\varphi_i \cdot \phi(2^n\varphi_i - p) \cdot \phi(2^n\varphi_i - p')] \ , \tag{55}$$

and

$$S_{g,mp'} = 2^{n/2} \sum_{i=1}^{I} \frac{h}{2} [\phi(2^n\varphi_{i-1} - p') \cdot S_{g,m}(r,\varphi_{i-1}) + \phi(2^n\varphi_i - p') \cdot S_{g,m}(r,\varphi_i)] \ . \tag{56}$$

The mesh size h is determined by the wavelet construction distance d (taken as 2^{-8}) and dilation order n; i.e., $h = d/2^n$. As a preprocessing step, all the integrations are calculated only once before the source iteration.

The angular discretized form of the neutron transport equation, as in Eq. (50), is a coupled partial differential equation set with only spatial variables. There are many numerical methods to solve it. Here, we choose the least-squares finite element method (FEM) to discretize the spatial variables in Eq. (50). Wu and Ju[14] developed a least-squares FEM code that uses both rectangular and triangular meshes for different geometries. The least-squares finite element variational formulation of Eq. (50) can be written as

$$\begin{aligned} &\iint \left(D_{x,mp'p'} \frac{\partial \psi_{g,mp'}}{\partial x} + D_{y,mp'p'} \frac{\partial \psi_{g,mp'}}{\partial y} + \Sigma_t \psi_{g,mp'} \right) \left(D_{x,mp'p'} \frac{\partial \psi^0}{\partial x} + D_{y,mp'p'} \frac{\partial \psi^0}{\partial y} + \Sigma_t \psi^0 \right) dxdy \\ &= \iint \left(S_{g,mp'} - \sum_{p=1,\, p\neq p'}^{P} \left(D_{x,mpp'} \frac{\partial \psi_{g,mp}}{\partial x} + D_{y,mpp'} \frac{\partial \psi_{g,mp}}{\partial y} \right) \right) \\ &\quad \times \left(D_{x,mp'p'} \frac{\partial \psi^0}{\partial x} + D_{y,mp'p'} \frac{\partial \psi^0}{\partial y} + \Sigma_t \psi^0 \right) dxdy \ , \end{aligned} \tag{57}$$

where $\psi_{g,mn} \in V$ and all admissible $\psi^0 \in V$; V is a subspace in Hilbert space H^1. Here, an iteration process is added to calculate the wavelet expansion coefficients $\psi_{g,mp}$ one by one.

The vacuum boundary condition and the reflective boundary condition are given respectively as

$$\Phi_g(r_b, \Omega^{q^{in}}) = 0 \tag{58}$$

and

$$\Phi_g(r_b, \Omega^{q^{in}}) = \Phi_g(r_b, \Omega^{q^{ref}}) \ , \tag{59}$$

where q^{in} and q^{ref} denote the incident quadrant and reflective quadrant, respectively, according to the location of the boundary. In DWM, Eqs. (58) and (59) are rewritten in terms of the wavelet expansion coefficients as

$$\psi_{g,mp}^{q^{in}}(r_b) = 0 \ , \quad m = 1, M \text{ and } p = 1, P \tag{60}$$

and

$$\psi_{g,mp}^{q^{in}}(r_b) = \psi_{g,mp}^{q^{ref}}(r_b) \ , \quad m = 1, M \text{ and } p = 1, P \ . \tag{61}$$

III.B. Accelerations of DWM in X-Y Geometry

In this section, the accelerations are introduced to the DWM solution. They are based on the within-group equation[15]

$$\begin{aligned} &(\Omega\nabla + \Sigma_t)\Phi_g(r,\Omega) - \int d\Omega'\, \Sigma_{gg}(r, \Omega\cdot\Omega')\Phi_g(r,\Omega') \\ &\quad = S_g^e(r,\Omega) \ , \end{aligned} \tag{62}$$

where

$$S_g^e(r,\Omega) = q_{f,g}(r,\Omega) + q_{ex,g}(r,\Omega) + \sum_{g' \neq g} \int d\Omega'\, \Sigma_{gg'}(r, \Omega\cdot\Omega')\Phi_{g'}(r,\Omega') \ , \tag{63}$$

and the iteration scheme is written as

$$(\Omega\nabla + \Sigma_t)\Phi_g^{l+1/2}(r,\Omega) = S_g^e(r,\Omega) + \int d\Omega'\, \Sigma_{gg}(r,\Omega\cdot\Omega')\Phi_g^l(r,\Omega') \ , \tag{64}$$

where l denotes the iteration index.

First, CMR (Ref. 15) is applied. The CMR acceleration method is extremely simple to apply regardless of the discretization scheme for the transport equation.

By performing angular integration and spatial integration over coarse mesh cell i, we obtain the following rebalance equation:

$$\sum_{i'} \int_{\Gamma_{ii'}} d\Gamma\, J_{g,i}^{+} - \sum_{i'} \int_{\Gamma_{ii'}} d\Gamma\, J_{g,i}^{-} + \int_{V_i} dV \Sigma_{r,g,i}\bar{\Phi}_{g,i} = \int_{V_i} dV\, S_{g,i}^e \ , \tag{65}$$

where i' is the index of a neighboring coarse mesh cell and $\Sigma_{r,g}$ is the removal cross section defined as

$$\Sigma_{r,g} = \Sigma_{t,g} - \Sigma_{s,gg} \ . \tag{66}$$

$J_g^{\pm}$ denotes the emergent and incident current along the normal direction of the coarse mesh cell, and $\bar{\Phi}_g$ is the average scalar flux in the coarse mesh cell. In DWM, the current is formulated as follows:

$$J_{g,x}^{+} = \sum_{q^{out}} \int_{-1}^{1} \sqrt{1-\mu^2}\, d\mu \int_{\varphi\in q^{out}} |\cos\varphi|\cdot\Phi_g(\mu,\varphi)\, d\varphi \ , \tag{67}$$

$$J_{g,y}^{+} = \sum_{q^{out}} \int_{-1}^{1} \sqrt{1-\mu^2}\, d\mu \int_{\varphi\in q^{out}} |\sin\varphi|\cdot\Phi_g(\mu,\varphi)\, d\varphi \ , \tag{68}$$

$$J_{g,x}^{-} = \sum_{q^{in}} \int_{-1}^{1} \sqrt{1-\mu^2}\, d\mu \int_{\varphi\in q^{in}} |\cos\varphi|\cdot\Phi_g(\mu,\varphi)\, d\varphi \ , \tag{69}$$

and

$$J_{g,y}^{-} = \sum_{q^{in}} \int_{-1}^{1} \sqrt{1-\mu^2}\, d\mu \int_{\varphi\in q^{in}} |\sin\varphi|\cdot\Phi_g(\mu,\varphi)\, d\varphi \ , \tag{70}$$

where q^{in} and q^{out} stand for the incident and emergent quadrants, respectively, according to the given boundary.

Then, the updated angular flux in coarse mesh cell i is given as

$$\Phi_g^{l+1}(r,\mu,\varphi) = f_i \Phi_g^{l+1/2}(r,\mu,\varphi) \ , \quad r \in i \ , \tag{71}$$

and the CMR equation is derived easily as

$$\left[\sum_{i'} \int_{\Gamma_{ii'}} d\Gamma\, J_{g,i}^{+,l+1/2} + \int_{V_i} dV \Sigma_{r,g,i}\bar{\Phi}_{g,i}^{l+1/2}\right] f_i - \sum_{i'} \int_{\Gamma_{ii'}} d\Gamma\, J_{g,i'}^{-,l+1/2} f_{i'} = \int_{V_i} dV\, S_{g,i}^e \ . \tag{72}$$

The second method for acceleration is the CMFD method.[16,17] Different from CMR, the form of the CMFD equations is similar to that of the usual finite difference equation with cell-centered unknowns, but there is an additional current correction factor.

In the CMFD method, the regional cross sections and scalar fluxes are calculated as

$$\bar{\Sigma}_{rg,i} = \frac{\sum_{k\in i} V_k \Sigma_{rg,k}\bar{\Phi}_{g,k}}{\bar{\Phi}_{g,i} V_i} \tag{73}$$

and

$$\bar{D}_{g,i} = \frac{\bar{\Phi}_{g,i} V_i}{3\sum_{k\in i} V_k \Sigma_{tg,k}\bar{\Phi}_{g,k}} \ , \tag{74}$$

where

$$\bar{\Phi}_{g,i} = \frac{\sum_{k\in i} V_k \bar{\Phi}_{g,k}}{V_i} \quad \text{and} \quad V_i = \sum_{k\in i} V_k \ , \tag{75}$$

where $\bar{\Phi}_{g,k}$ is the scalar flux of fine mesh cell k in the coarse mesh cell i.

The current correction factor $\hat{D}_{g,i}$ is defined as

$$\hat{D}_{g,i} = -\frac{J_{g,i} + \tilde{D}_{g,i}(\bar{\Phi}_{g,i+1} - \bar{\Phi}_{g,i})}{\bar{\Phi}_{g,i+1} + \bar{\Phi}_{g,i}} \ , \tag{76}$$

where $\tilde{D}_{g,i}$ is given as

$$\tilde{D}_{g,i} = 2\,\frac{(D_{g,i}/h_i)(D_{g,i+1}/h_{i+1})}{D_{g,i}/h_i + D_{g,i+1}/h_{i+1}} \tag{77}$$

and $J_{g,i}$ is the net current at the interface of nodes that are supplied by the fine mesh calculation of DWM. Different from CMR, here the current is defined, for each group, as

$$J_{g,x} = \sum_q \int_{-1}^{1} \sqrt{1-\mu^2}\, d\mu \int_{\varphi \in q} \cos\varphi \cdot \Phi_g(\mu,\varphi)\, d\varphi \tag{78}$$

and

$$J_{g,y} = \sum_q \int_{-1}^{1} \sqrt{1-\mu^2}\, d\mu \int_{\varphi \in q} \sin\varphi \cdot \Phi_g(\mu,\varphi)\, d\varphi \ , \tag{79}$$

where q is the total quadrants according to the dimension of calculation.

Define the updated angular flux in coarse mesh i as

$$\Phi_g^{l+1}(r,\mu,\varphi) = \frac{\bar{\Phi}_g^{l+1}(r)}{\bar{\Phi}_g^{l+1/2}(r)} \Phi_g^{l+1/2}(r,\mu,\varphi) \ , \quad r \in i \ . \tag{80}$$

The CMFD equation for coarse mesh cell i is written as

$$\begin{aligned} &-\sum_{i'} \int_{\Gamma_{ii'}} d\Gamma (\tilde{D}_{i\pm 1/2} \pm \hat{D}_{i\pm 1/2}) \bar{\Phi}_{g,i'}^{l+1} \\ &\quad + \left(\sum_i \int_{\Gamma_{ii'}} d\Gamma (\tilde{D}_{i\pm 1/2} \mp \hat{D}_{i\pm 1/2}) + \int_{V_i} dV \Sigma_{r,g,i} \right) \bar{\Phi}_{g,i}^{l+1} \\ &\quad = \int_{V_i} dV S_{g,i}^{e} \ , \end{aligned} \tag{81}$$

where i' is the index of a neighboring coarse mesh cell.

From Eqs. (71) and (72) in the case of CMR, and Eqs. (80) and (81) in the case of CMFD, we obtain the updated angular flux of energy group g to provide the within-group scattering source in the $l+1$ iteration in the transport equation.

IV. NUMERICAL TESTS AND RESULTS

Previous works[8,9] indicated that DWM with the polar S_N and one-dimensional piecewise Daubechies' scaling function expansion scheme in the azimuthal angle is the most efficient and stable form among the options of using Daubechies' wavelets in the angular discretization. Therefore, it is determined as the final form of DWM.

In this paper, the method is verified against the MOC code CRX, and additional calculations are done to reveal the effect of different orders in the angular discretization, the performance in a ray-effect problem, and the validity and effectiveness of acceleration methods in the wavelet-based angular discretization scheme. Also, a set of case calculations is performed on a multicell structure problem with a void region and different fuel loadings to demonstrate the efficacy of DWM.

IV.A. Adams' Problem

This is a two-region fixed-source problem that was studied by Adams.[6] The geometry is shown in Fig. 4, and the cross sections are given in Table III. Reflective boundary conditions are given in all sides. Figure 5 illustrates the reference angular flux distribution (at a latitude of $\mu = 0.33$) at the given spatial point. It is irregular, peaky, and discontinuous. In view of the capability of DWM in representing the complicated azimuthal angular structure, this problem is solved by DWM.

By using DWM, we obtained the angular flux distribution along the azimuthal direction at a latitude of $\mu = 0.5774$. Because of the difference of polar discretization, here the comparison focuses on the angular distribution rather than on the exact amplitude of the angular flux. Figure 6 illustrates the angular distributions obtained by DWM using Daubechies order $N = 2$. Higher dilation order provides more accurate results of the angular flux distribution.

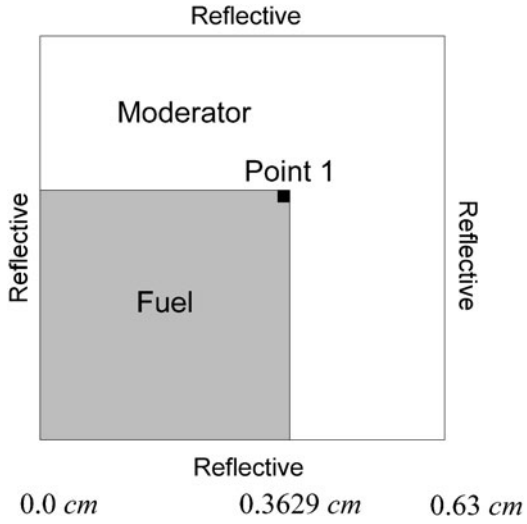

Fig. 4. Geometry of Adams' problem.

TABLE III

Cross Sections of Adams' Problem

	Source ($cm^{-3}\ s^{-1}$)	Σ_t (cm^{-1})	Σ_s (cm^{-1})
Fuel	2π	0.141367	0.057843
Moderator	0.0	0.072774	0.008642

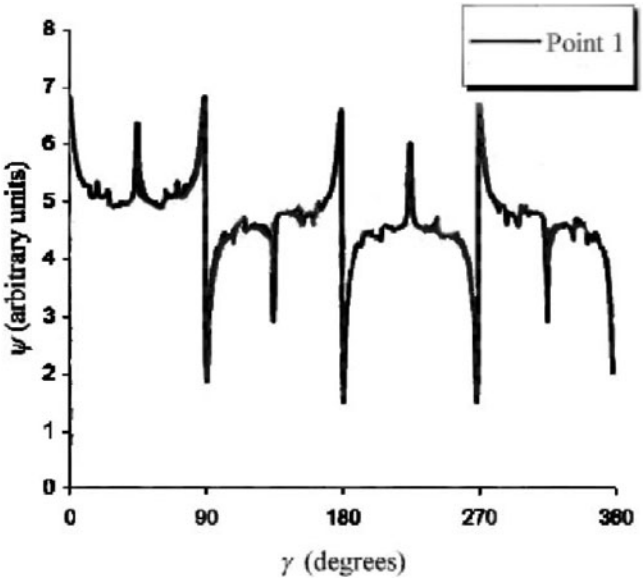

Fig. 5. Angular flux distribution from Adams[6] with 512 quadrature points.

TABLE IV

Comparison of Regionwise Average Scalar Fluxes of Adams' Problem

Region		Fuel	Moderator
$n = 3$[a,b]	$N = 2$[c]	30.019	29.213
	$N = 4$	30.266	29.072
$n = 4$	$N = 2$	30.218	29.102
	$N = 4$	30.344	29.021
$n = 5$	$N = 2$	30.315	29.041
	$N = 4$	30.365	29.008
$n = 6$	$N = 2$	30.333	29.029
	$N = 4$	30.372	29.003
CRX	(64,8)[d]	30.294	29.062
	(32,8)[e]	30.273	29.076

[a]Dialation order n in DWM.
[b]Four polar angles, 2^n azimuthal unknowns per quadrant, 121 rectangular meshes.
[c]Daubechies order N in DWM.
[d](64,8) angles per quadrant, 128 rays per unit cell (0.63 × 0.63 cm).
[e](32,8) angles per quadrant, 128 rays per unit cell (0.63 × 0.63 cm).

Figure 7 gives the comparison of angular distributions for the Daubechies order $N = 4$. Compared with the distributions obtained from low Daubechies order, we note that the ones with higher Daubechies order perform well even for the low dilation order. This is because the basis function with higher Daubechies order is smoother and more symmetric, as illustrated in Fig. 1b. However, for higher dilation order, the results using different Daubechies orders become closer. In addition, a comparison of angular fluxes at point 1 for an azimuthal angle of 45 deg is given in Fig. 8 to visually indicate its convergence. With increase of the dilation order, the angular flux tends to be convergent, however, with a slow rate. This is due to the singular variation of the angular flux in this problem.

Moreover, even for dilation order $n = 5$, the number of unknowns to be determined is only 128 for a single polar angle. Compared with hundreds of unknowns in the S_N method,[6] we may say that DWM is more efficient in representing complicated angular distributions.

Table IV gives the quantitative comparison of average scalar fluxes between DWM and CRX, which demonstrates that the results of DWM are accurate and reliable.

IV.B. Ray-Effect Problem

This problem (originally known as the Watanabe-Maynard Problem) is taken from Ref. 18 to verify the accuracy of DWM for a ray-effect problem. This is a fixed-source problem consisting of a void region and a highly scattering medium. Figure 9 illustrates the geometry and the cross sections. Figure 10a is a copy from Ref. 18 that provides reference solutions by an integral transport theory method with several tracking parameters. Figures 10b and 10c give the wavelet-based solutions with different Daubechies orders N, respectively.

DWM uses a piecewise continuous approximation to the angular flux. This kind of method tends to mitigate ray effects. However, unlike the P_N method, DWM has no complete rotational symmetry. Therefore, DWM cannot eliminate ray effects completely. Based on the comparison of scalar flux distributions, it is ascertained that ray effects arise in the wavelet-based angular discretization scheme with low Daubechies order and dilation order, although much weaker than in the reference solutions using low tracking order. However, higher Daubechies order and dilation order mitigate ray effects significantly, because of their longer compact support and better symmetry. Comparison of the solutions with different polar orders indicates that ray effects are not sensitive to the polar discretization.

IV.C. Accelerations in DWM

This problem is designed to test the effectiveness of the acceleration methods implemented in DWM. The geometry is illustrated in Fig. 11, together with the fine mesh divisions. Two-group cross sections of the fuel and moderator are shown in Table V. Reflective boundary conditions are given in all sides.

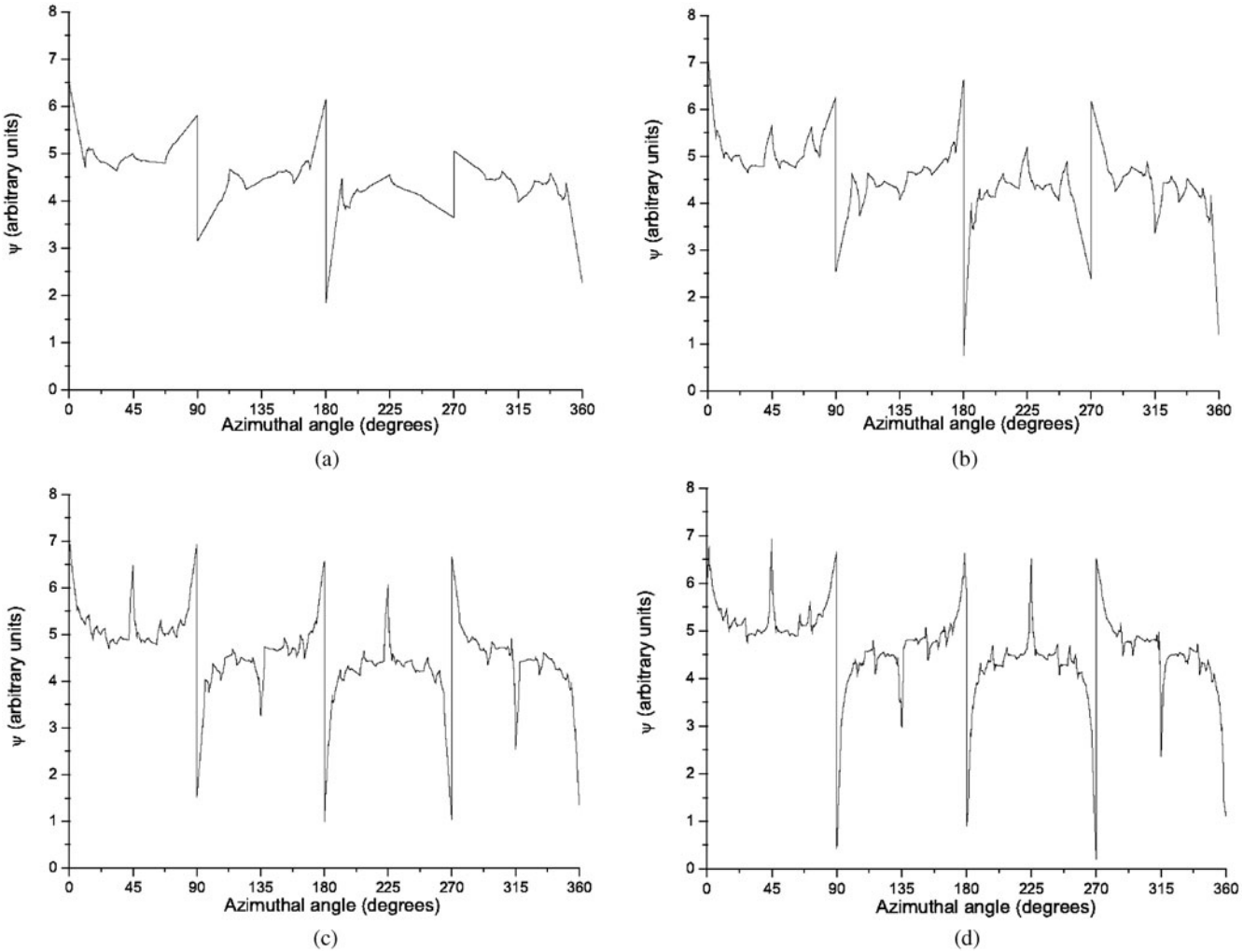

Fig. 6. Angular flux distribution at point 1 for (a) $N = 2$ and $n = 3$, (b) $N = 2$ and $n = 4$, (c) $N = 2$ and $n = 5$, and (d) $N = 2$ and $n = 6$.

TABLE V

Cross Sections of the Problem in Fig. 10

		$\nu\Sigma_f$ (cm^{-1})	$\Sigma_{1\text{-}1}$ (cm^{-1})	$\Sigma_{1\text{-}2}$ (cm^{-1})	Σ_t (cm^{-1})	χ
Group 1	Fuel	0.006203	0.178000	0.010020	0.196647	1.0
	Moderator	0.000000	0.199500	0.021880	0.222064	
Group 2	Fuel	0.110100	0.001089	0.525500	0.596159	0.0
	Moderator	0.000000	0.001558	0.878300	0.887874	

Table VI gives a comparison between the original source iteration solution and acceleration solutions using CMR and CMFD. For the within-group iteration, the criterion used is 10^{-3}, and no more than ten iterations are required for all calculations. The stop criterion used for k_{eff} is 10^{-5}. From the results, we note that both the CMR and CMFD are effective to accelerate DWM, if the size of the coarse mesh cells is relatively

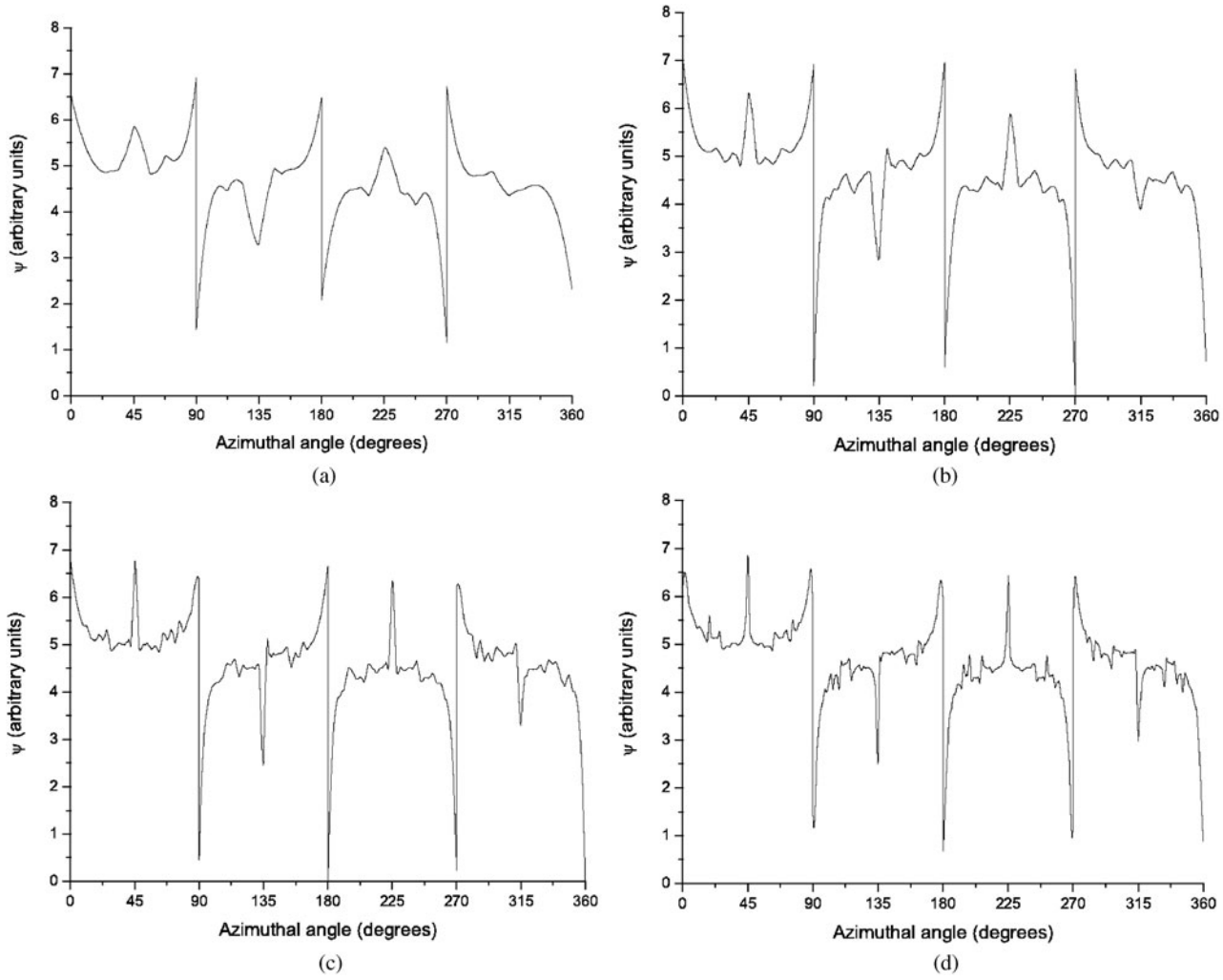

Fig. 7. Angular flux distribution at point 1 for (a) $N = 4$ and $n = 3$, (b) $N = 4$ and $n = 4$, (c) $N = 4$ and $n = 5$, and (d) $N = 4$ and $n = 6$.

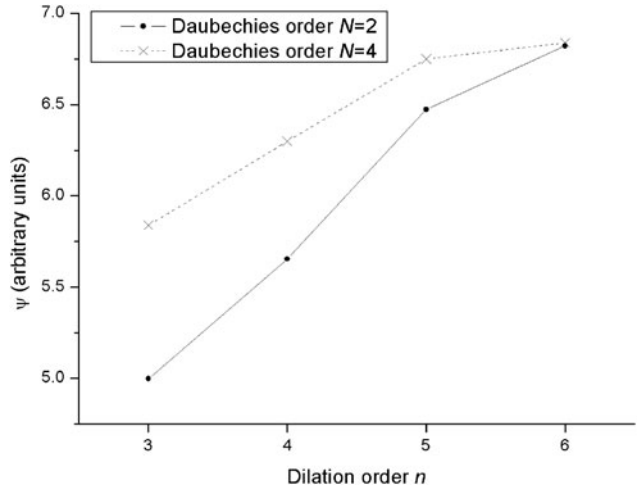

Fig. 8. Comparison of angular fluxes for several wavelet orders at point 1 for 45-deg azimuthal angle.

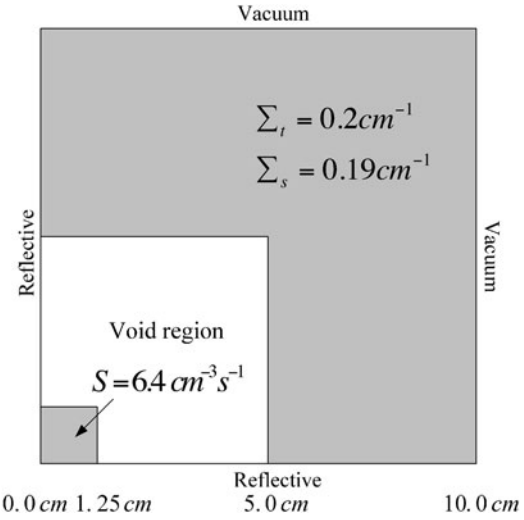

Fig. 9. Description of the ray-effect problem.

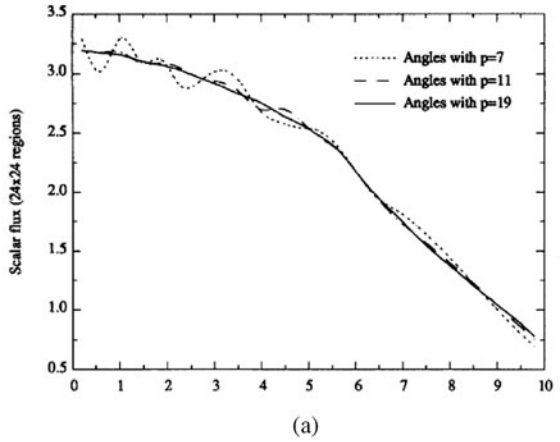

(a)

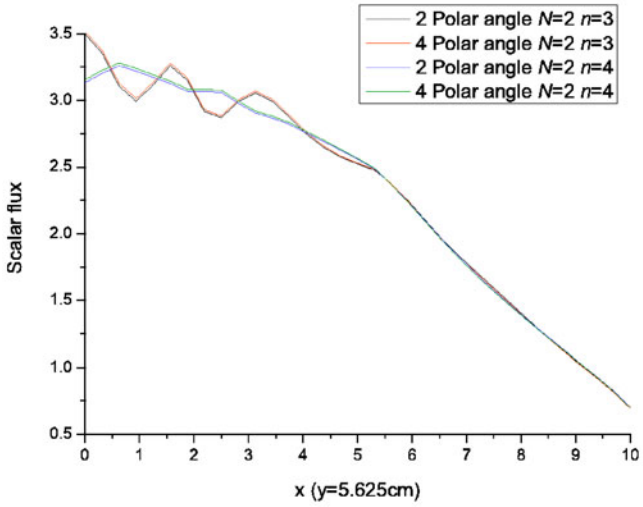

(b)

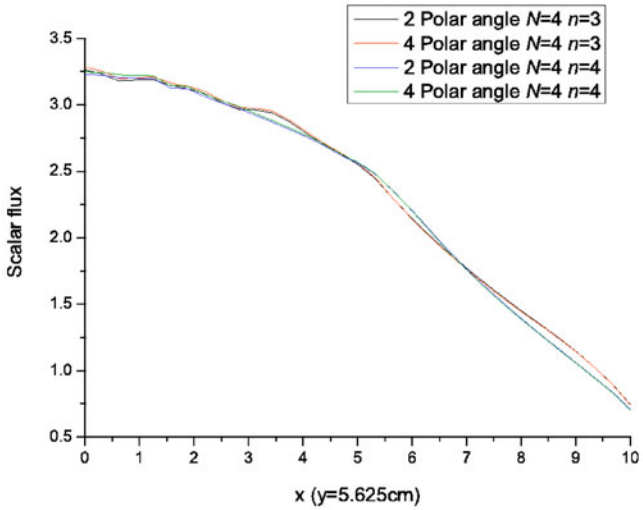

(c)

Fig. 10. Scalar flux distribution along $y = 5.625$ cm (a) in the reference solutions,[18] (b) using Daubechies order $N = 2$, and (c) using Daubechies order $N = 4$.

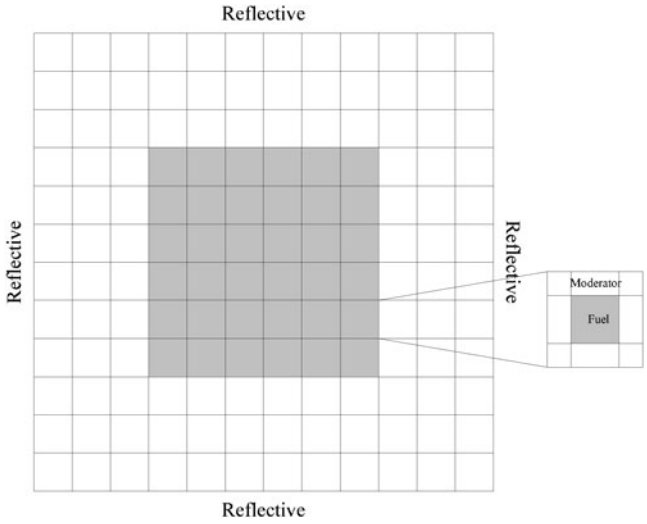

Fig. 11. Geometry of the acceleration test problem.

large. However, with refinement of coarse meshes, CMFD becomes more effective, while CMR loses effectiveness and eventually becomes nonconverging.

IV.D. Test of DWM in a Multicell Problem

A series of calculations is performed with DWM on a multicell structure problem. A pin cell lattice consists of a fuel rod and moderator. Four cell lattices construct the multicell structure as illustrated in Fig. 12. The reflective boundary conditions are given at the left and bottom sides, while the vacuum boundary conditions are given at the top and right sides. Five cases are considered with three types of pin cells: UO_2 fuel cell, mixed oxide (MOX) fuel cell, and void cell in which the fuel rod position is made empty. Detailed descriptions of the cases are illustrated in Fig. 13. Two-group cross sections used are given in Table VII.

All calculations are based on quadratic triangular mesh cells with a total of 504 finite elements and 1081 nodes. The same angular discretization is applied, where the Daubechies order N is equal to 2, dilation order n is equal to 3, and four discrete polar angles are used in the upper hemisphere. Reference solutions are given by using the CRX code, which is based on MOC. Table VIII gives a detailed comparison between the wavelet-based solutions and reference solutions. The results indicate that they are in good agreement and DWM is versatile in handling a variety of transport problems. As for computer memory, this test problem requires >470 MB, and >90% of the requirement is used to store the stiffness matrix of every energy group and direction in the FEM solution process.

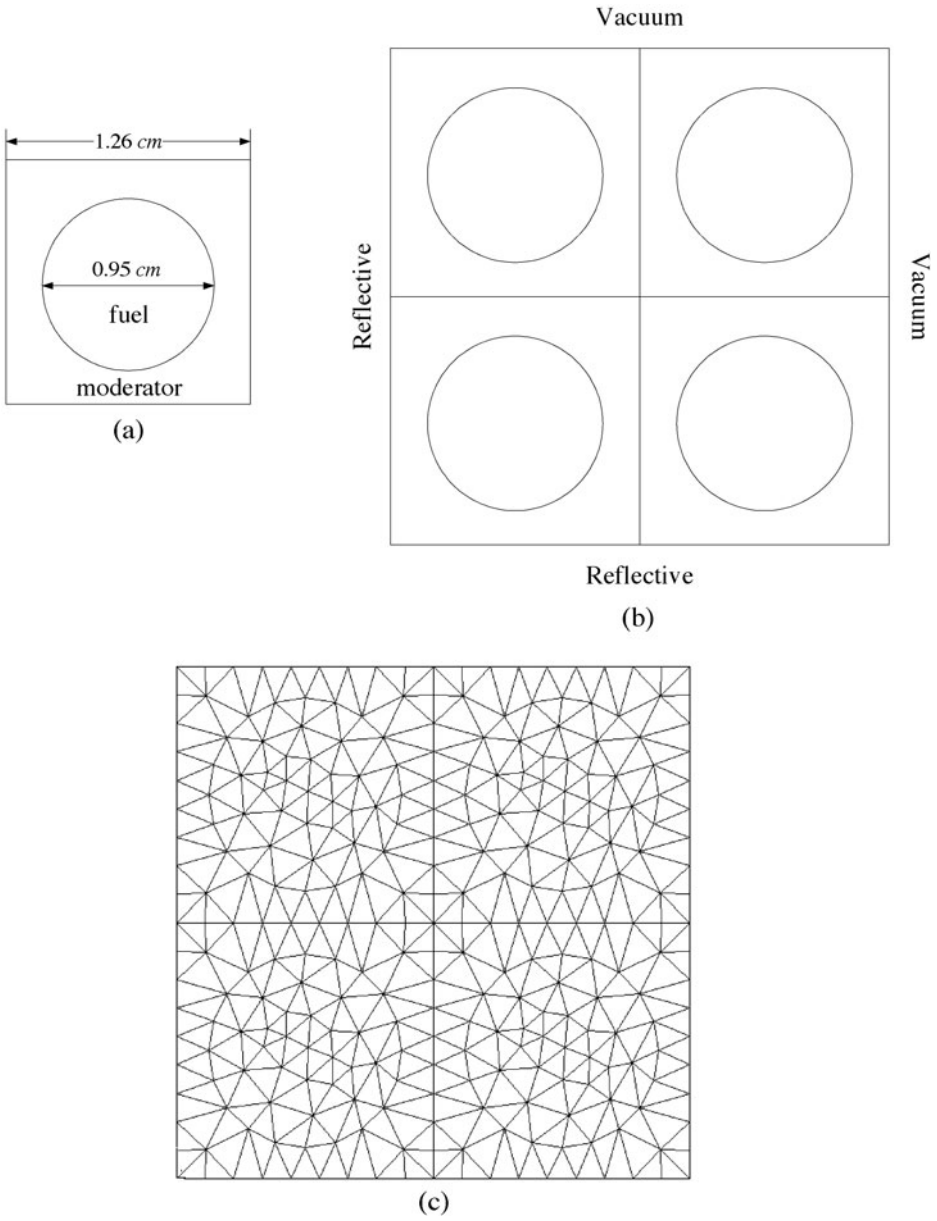

Fig. 12. Configuration of (a) pin cell, (b) multicell, and (c) computational finite element meshes (triangular meshes) for the multicell.

V. CONCLUSIONS

We have described a new method discretizing the angular variables in the neutron transport equation, which uses the Daubechies' scaling function as the basis function for expanding the azimuthal variable. The polar variable is discretized by using discrete ordinates in a decoupled form. In particular, the construction of Daubechies' wavelets on an interval is used to remove the edge effect between subdomains in the angular variable. The good localization properties of Daubechies' wavelets suggest that they have strong potential for high-order angular approximations of irregular and challenging problems.

The results of the benchmark problems tested so far indicate that in general larger dilation order provides more accurate solutions with fixed Daubechies order. Meanwhile, there are almost no differences between different Daubechies orders if the dilation order is high enough. The acceleration methods implemented in DWM are demonstrated to be both feasible and effective by

TABLE VI

Comparison of Acceleration Effects in DWM

	k_{eff}	Maximum Relative Error in Flux (%)		Number of Outer Iterations	CPU Time	Speedup
		Fuel	Moderator			
SI	0.7831	—	—	87	89.50	—
CMR						
2×2[a]	0.7830	0.0048	0.0256	14	14.14	6.33
3×3	0.7830	0.0048	0.0252	24	18.88	4.74
4×4	0.7830	0.0048	0.0247	67	46.25	1.94
6×6	N. C.[b]	N. C.	N. C.	N. C.	N. C.	N. C.
CMFD						
2×2	0.7830	0.0048	0.0256	14	14.92	6.00
3×3	0.7830	0.0042	0.0252	10	11.00	8.14
4×4	0.7830	0.0048	0.0247	8	9.06	9.88
6×6	0.7830	0.0042	0.0247	6	6.98	12.82

[a]Number of coarse mesh cells.
[b]N.C. is not convergent.

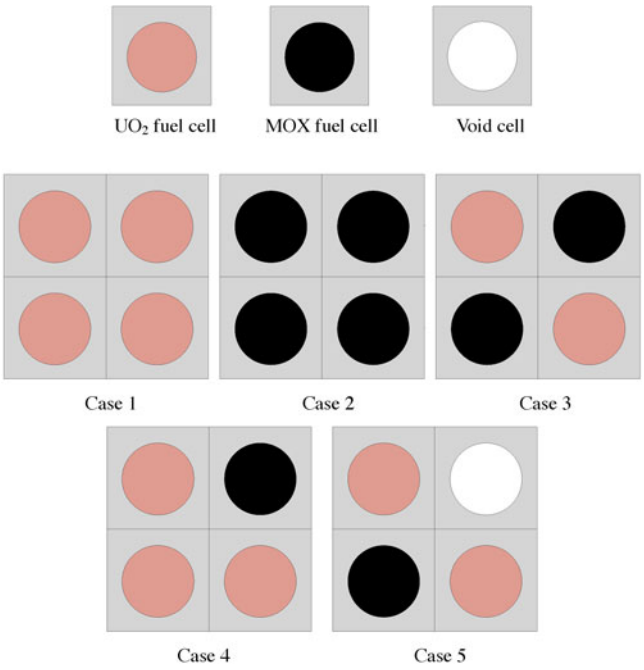

Fig. 13. Three types of pin cell and five cases of the multicell structure problem.

TABLE VII

Cross Sections of the Multicell Structure

	Σ_t	$\nu\Sigma_f$	Σ_a	$\Sigma_{s\to1}$	$\Sigma_{s\to2}$
Cross Sections of UO_2 Fuel					
Group 1	0.196647	0.006203	0.008627	0.178000	0.010020
Group 2	0.596159	0.110100	0.069570	0.001089	0.525500
Cross Sections of MOX Fuel					
Group 1	0.379246	0.036451	0.033866	0.344903	0.000477
Group 2	1.149943	0.938410	0.745568	0.000000	0.404375
Cross Sections of Void					
Group 1	0.000000	0.000000	0.000000	0.000000	0.000000
Group 2	0.000000	0.000000	0.000000	0.000000	0.000000
Cross Sections of Moderator					
Group 1	0.237672	0.000000	0.000493	0.213045	0.024135
Group 2	0.864320	0.000000	0.009913	0.000779	0.853628

the numerical tests. Compared with CMR, CMFD behaves more stably with the refinement of coarse meshes in the wavelet-based angular discretization scheme.

The test results also indicate that DWM is capable of treating transport problems exhibiting angularly complicated behaviors, effective in mitigating (if not eliminating) ray effects and versatile in handling transport phenomena in a variety of structured media.

As future work, investigations of alternative spatial treatments are warranted in order to further reduce the computational demands and memory requirements of the scheme (presently done by the FEM in this study).

TABLE VIII

Comparisons Between the Wavelet-Based Solutions and Reference Solutions

		k_{eff}	CPU Time (s)	Fast Flux[a]		Thermal Flux[a]	
				Fuel[b]	Moderator	Fuel	Moderator
Case 1	CRX	0.0267	0.63[c]	1.0000	0.8389	0.0768	0.0781
	DWM	0.0268	550[c]	1.0000	0.8421	0.0798	0.0813
Case 2	CRX	0.1063	0.52	1.0000	0.8446	0.0228	0.0319
	DWM	0.1068	355	1.0000	0.8473	0.0233	0.0328
Case 3	CRX	0.0789	0.58	1.0000	0.7740	0.0250	0.0345
	DWM	0.0795	379	1.0000	0.7785	0.0257	0.0357
Case 4	CRX	0.0464	0.49	1.0000	0.9000	0.0858	0.0840
	DWM	0.0470	523	1.0000	0.9074	0.0869	0.0889
Case 5	CRX	0.0680	1.52	1.0000	0.7471	0.0228	0.0316
	DWM	0.0687	372	1.0000	0.7502	0.0236	0.0329

[a]Average scalar flux in the fuel pin cell at the left bottom corner.
[b]Flux is normalized such that fast flux in the fuel region is unity.
[c]On Intel Xeon 3.06 GHz.

ACKNOWLEDGMENTS

This research was supported in part by financial support of the National Science Foundation of China (approval numbers 10605017 and 10875094) and the Korea Science and Engineering Foundation. This work started while the third author (L. Cao) stayed at Korea Advanced Institute of Science and Technology (KAIST) in 2005–2006 and was continued by the first author (Y. Zheng) working at Xi'an Jiaotong University in 2006–2008 and during a visit to KAIST in 2008–2009. The authors appreciate the help of H. J. Yoo of KAIST, who provided reference solutions to some of the problems presented in this paper.

REFERENCES

1. A. KADEM, "Solving Transport Equation via Walsh Function and Sumdu Transform," *Appl. Comput. Math.*, **7**, 107 (2008).

2. A. YILMAZER, "Jacobi Polynomials Approximation to the One-Speed Neutron Transport Equation," *Ann. Nucl. Energy*, **34**, 977 (2007).

3. A. G. BUCHAN et al., "Linear and Quadratic Octahedral Wavelets on the Sphere for Angular Discretisations of the Boltzmann Transport Equation," *Ann. Nucl. Energy*, **32**, 1224 (2005).

4. A. G. BUCHAN et al., "Self-Adaptive Spherical Wavelets for Angular Discretizations of the Boltzmann Transport Equation," *Nucl. Sci. Eng.*, **158**, 244 (2008).

5. I. DAUBECHIES, *Ten Lectures on Wavelets*, Society for Industrial and Applied Mathematics, Philadelphia, Pennsylvania (1992).

6. M. L. ADAMS, "Angular Dependence of the Fast Flux in Reactor Lattices," *Trans. Am. Nucl. Soc.*, **84**, 212 (2001).

7. M. A. SMITH et al., "Comparison of Angular Approximations for PWR Cell Calculations," *Trans. Am. Nucl. Soc.*, **84**, 90 (2001).

8. N. Z. CHO and L. CAO, "Wavelet-Theoretic Method for Solution of Neutron Transport Equation," *Trans. Korean Nuclear Society Spring Mtg.*, Chuncheon, Korea, May 25–26, 2006.

9. L. CAO, H. WU, and Y. ZHENG, "Solution of Neutron Transport Equation Using Daubechies' Wavelet Expansion in the Angular Discretization," *Nucl. Eng. Des.*, **238**, 2292 (2008).

10. S. G. HONG and N. Z. CHO, "CRX: A Code for Rectangular and Hexagonal Lattices Based on the Method of Characteristics," *Ann. Nucl. Energy*, **25**, 547 (1998).

11. D. E. NEWLAND, *An Introduction to Random Vibrations, Spectral & Wavelet Analysis*, John Wiley and Sons, New York (1993).

12. A. COHEN, I. DAUBECHIES, and P. VIAL, "Wavelets on the Interval and Fast Wavelet Transforms," *Appl. Comput. Harmonic Anal.*, **1**, 54 (1993).

13. G. BELL and S. GLASSTONE, *Nuclear Reactor Theory*, Litton Educational Publishing, New York (1970).

14. H. WU and H. JU, "A Least-Square Finite-Element S_N Method for Solving First-Order Neutron Transport Equation," *Nucl. Eng. Des.*, **237**, 823 (2007).

15. E. E. LEWIS and W. F. MILLER, *Computational Method of Neutron Transport*, John Wiley and Sons, New York (1984).

16. K. S. SMITH and J. D. RHODES, "Full-Core, 2-D, LWR Core Calculation with CASMO-4E," *Proc. PHYSOR 2002*, Seoul, Korea, October 7–10, 2002 (CD-ROM).

17. N. Z. CHO and C. J. PARK, "A Comparison of Coarse Mesh Rebalance and Coarse Mesh Finite Difference Accelerations for the Neutron Transport Calculations," *Proc. Int. Conf. Nuclear Mathematical and Computational Sciences (M&C 2003)*, Gatlinburg, Tennessee, April 6–11, 2003, American Nuclear Society (2003) (CD-ROM).

18. R. ROY, "Anisotropic Scattering for Integral Transport Code-2, Cyclic Tracking and Its Application to XY Lattices," *Ann. Nucl. Energy*, **18**, 511 (1991).